Public Quarterly Report

Date of Report*:* 12th Quarterly Report-October 2025
Contract Number: 693JK322RA0001
Prepared for: US Pipeline and Hazardous Materials Safety Administration
Project Title: Rapid Ultraviolet (UV) Cured Adhesive for Gas Main Cured-in-Place-Lining (CIPL)
Prepared by: Progressive Pipeline Management
Contact Information: Casey Giambrone, cfg@progressivepipe.com, *631-339-3075*
For the quarterly period ending: September 30, 2025

1: Items Completed During this Quarterly Period:

Item #	***Task #***	***Activity/Deliverable***	***Title***	***Federal Cost***	***Cost Share***
46	39	Traffic Loading/fatigue & Parallel Excavation	Traffic Loading	$50,469.50	$50,469.50
49	40	Axial Loading (Thermal) and Tensile Pull	Axial Loading	$14,702.00	$14,702.00
50	41	Simulated corrosion pressure test	Simulated corrosion	$7,761.00	$7,761.00
51	7	12th Quarterly Status Report & Data Analysis	12th Quarterly Report	$13,680.00	$13,680.00

2: Items Not Completed During this Quarterly Period:

Item #	***Task #***	***Activity/Deliverable***	***Title***	***Federal Cost***	***Cost Share***
		N/A			

3: Project Financial Tracking During this Quarterly Period:

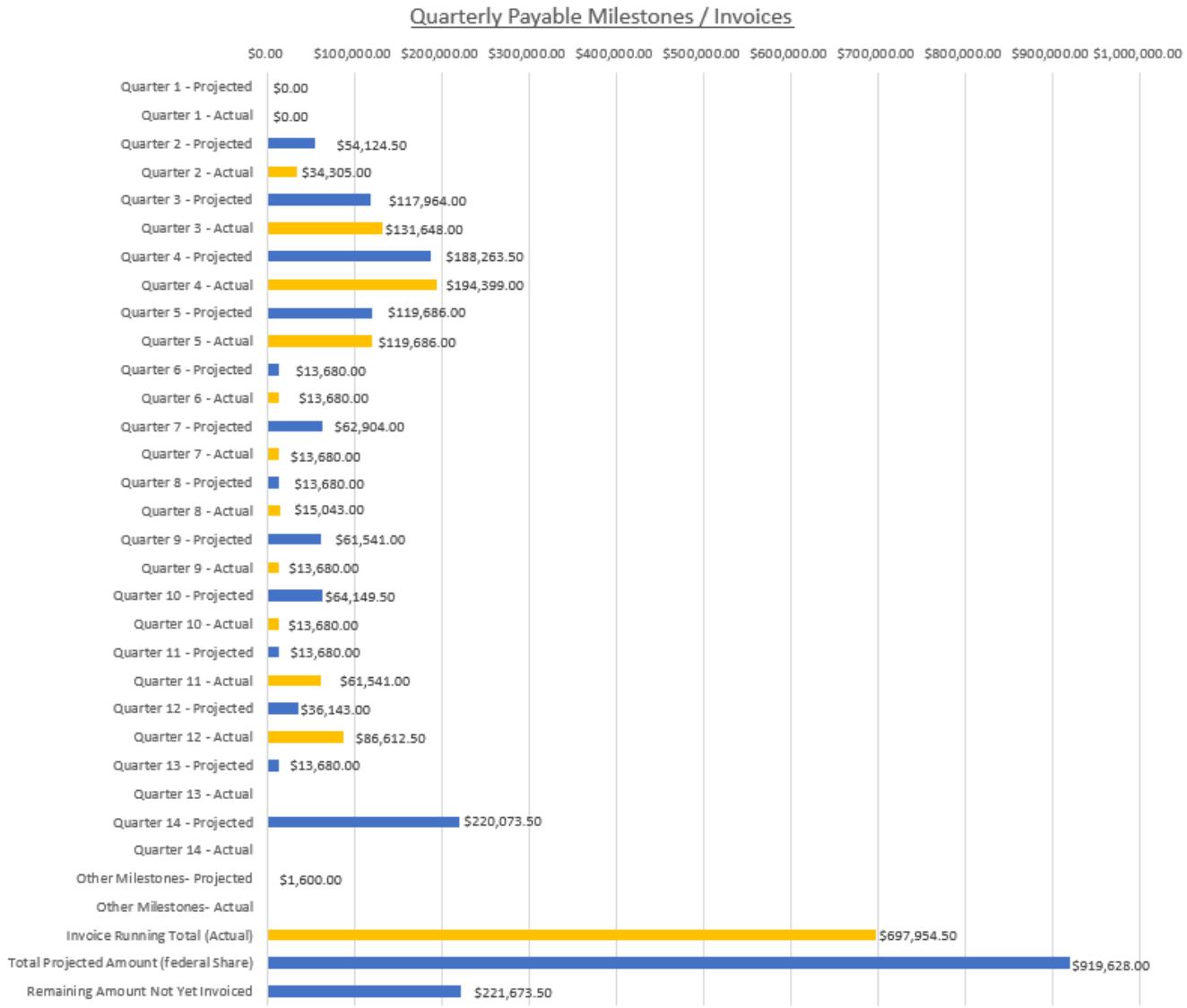

4: Project Technical Status –

6. Full-Scale Testing

Compared to the open trench method, trenchless technologies (TT) for water, wastewater, oil, and gas

pipelines are used increasingly to replace incident-prone legacy pipes. TT results in less environmental impact and the minimization of excavation activities (Allouche et al., 2014; Lu et al., 2020; Najafi, 2005; Vladeanu & Matthews, 2018). A TT approach has a cost advantage compared to open cut. For a pipe diameter less than or equal to 12 in. (300 mm,) it costs half as much to place an internal lining inside a host pipe than to replace the pipeline inside an open cut (Zhao & Rajani, 2002). There has been much effort to develop internal replacement pipe (IRP) technologies as well as the formal standards and related documents concerning these technologies (Pipeline Infrastructure Committee 2021; ASME PCC-2 Article 403 2018; ASTM F1216 2016a; ASTM F3182 2016b; ASTM F1743 2017; ASTM D5813 2018; ASTM F2207 2019a; AWWA Committee 2019). Nevertheless, there are some outstanding questions about IRP technologies, including long-term suitability and performance, practical considerations for external loads, and the role of adhesion in structural capacity and response. Legacy host pipes undergo various failure modes depending on the type of loading. Moreover, studies are lacking for the long-term response of deteriorated host pipes to internal and external loads (Dixon et al., 2023b; Fu et al., 2020).

This section addresses external loads affecting IRP technologies by implementing a soon-to-be-released testing methodology, ASTM F3777-25. It presents lab-based methods for evaluating IRP over a 50-year service life with repaired pipe specimens. The specimens studied featured the IRP material STARLINE2000^{TM}, provided by PPM (Progressive Pipeline Management), which has a successful track record in both laboratory testing and field applications. The external loads are traffic loading, ground movement due to adjacent excavations, and thermally-induced axial deformation of the repaired system. This report is a logical extension of earlier work performed at Cornell University (e.g., Jeon et al., 2004; Stewart et al., 2015), which developed an evaluation framework for cured-in-place liners (CIPLs) under external loads. The framework developed at Cornell University assumed negligible mechanical contribution (stiffness) of the liner to the pipeline response. This assumption was conservative and appropriate, considering the type of materials that were evaluated by Cornell researchers at the time. The prior framework has been updated to account for the stiffness of a repair pipe in the estimation of field deformation. The numerical and analytical methods to estimate the field deformation of an STARLINE2000^{TM} IRP are outlined briefly in this report. Detailed test methods and major results are presented. Important observations and various aspects of the testing are discussed.

9.1 Methodology of Testing Full-Scale Specimen

The following section describes the test methodology to simulate major aspects of the external loading of rehabilitated pipe over a 50-year service life in the field. The approach applies laboratory loading to mimic deformations applied by traffic loading, adjacent excavations, and seasonal temperature fluctuation.

9.1.1 Lateral Loading

9.1.1.1 Model Description

A "beam-on-springs" finite element (FE) model was developed in OpenSees for a buried cast iron pipeline subjected to traffic loading and soil displacements representative of adjacent excavation activity. The pipeline elements were represented by 3-in. (75-mm) long, 1D Euler-Bernoulli beam elements. A circumferential gap (also referred to as crack) was modeled by removing host pipe elements. For the cases in which an IRP repair was combined with the host pipe, the missing element or gap was replaced with a beam element with properties of the IRP material and length equal to the width of the gap opening. CI joints were modeled using rotational, shear, and axial springs. Soil was represented using soil springs with a hyperbolic force-displacement.

9.1.1.2 Traffic Loading

As described in detail by Klingaman et al., (2022), traffic loading was derived from an HS-20 design truck and was conservatively increased to 30 kips (130 kN). The resulting traffic load was assumed to be applied at the ground surface according to the Boussinesq stress distribution for a point load on a semi-infinite elastic medium. The stress calculated at a depth of 30 in. (762 mm) was multiplied by the vertically projected area of the pipe (diameter times element size) and discretely applied to each pipeline node in the FE model (Figure 9.1). Resulting pipe deformations (e.g., relative rotations) were recorded so that they could be applied in the lab.

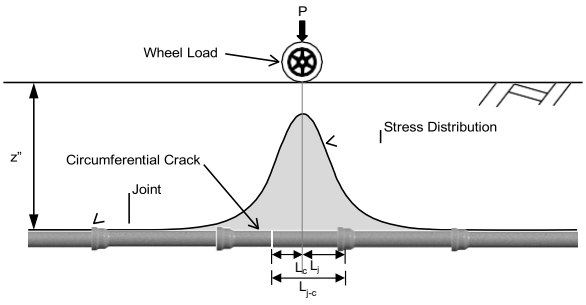

Figure 9.1: Schematic of traffic loading scenario

9.1.1.3 Adjacent Excavation

As described by Klingaman et al. (2024), soil displacement profiles were developed using a functional form proposed by Roboski & Finno (2006), which requires 3 inputs: excavation depth, H_e, maximum soil displacement, d_{max}, and the length over which d_{max} is developed, L. The adjacent excavation (AE) depth was assumed to be 20 ft. (6 m), various values of d_{max} were considered, ranging from 2.5-10 in. (63.5-254 mm), and L was assumed to be 50 ft. (15.2 m) (Figure 9.2). The soil displacements were applied to each soil node in the FE model and resulting rotations were recorded so that they could be applied in the lab. During this study, the smaller and larger parallel (adjacent) excavation events, typically referred to as PE1 and PE2 for each specimen, were associated with d_{max} of 2.5 in. (63.5 mm) and 5 in. (127 mm), respectively.

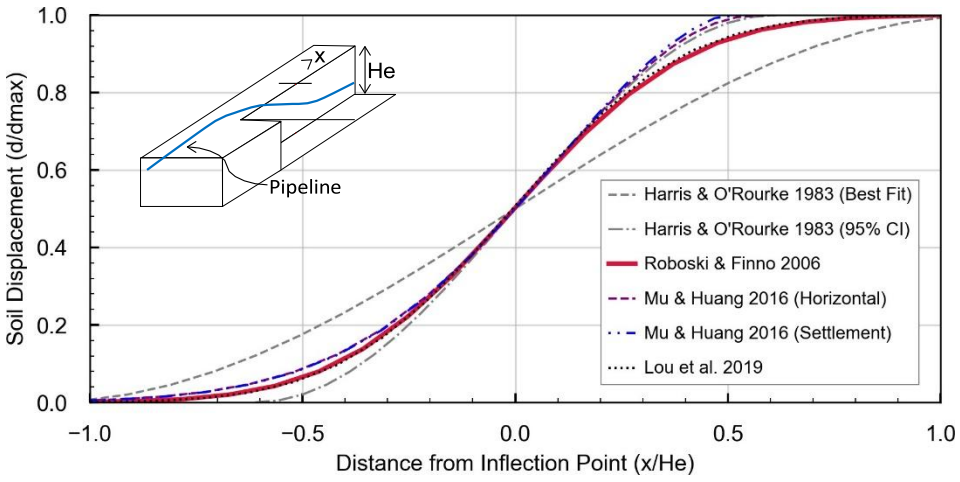

Figure 9.2: Soil displacement profiles parallel (adjacent) to an excavation from previous studies

9.1.2 Thermal Loading

Temperature fluctuations in soil will give rise to axial deformation and/or induced axial load in repaired systems from thermal expansion. Previous work used 40°F (22.2°C) as the annual soil temperature variation in New York State (Stewart et al., 2015). This work includes temperature variations of 40°F (22.2°C) and 50°F (27.8°C) and considers granular soil as the backfill material in contact with the host pipe. Additionally, this work considers the stress-free state of the system to be the highest temperature (T_{max}), such that all temperature variation is negative. To understand the problem, a mechanics-based analytical approach has been developed as shown in Figure 9.7 (Dixon et al., 2023a).

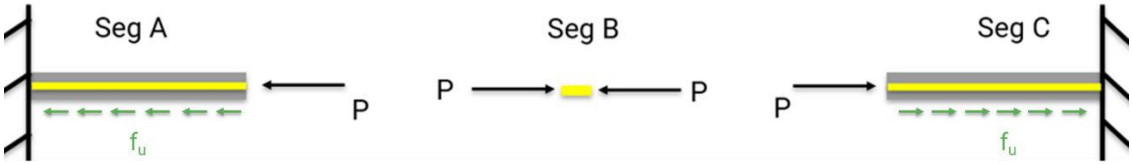

Figure 9.3: Fully bonded approach schematic with friction from pipe-soil interaction

The specimen is divided into three regions/segments: Segment A refers to the combined host and IRP section, and Segment B refers to the exposed IRP region (Segment C would refer to the other combined host and IRP section but symmetry allows the use of only Segment A and B). The host and repair pipe are treated as fully bonded in Segment A. Simple analytical expressions for the fully unbonded case are straightforward, and it is noted as the gap width (length of Segment B) approaches the system length, induced loads calculated with a fully-bonded assumption approach those for the unbonded case. Furthermore, even in "unbonded" systems, some level of intimate mechanical contact is necessary for a successful installation. So the initial assumption will be fully bonded (if results from initial assessments with small levels of axial displacement demonstrate a fully unbonded system, then the unbonded approach will be used). In this approach Segment A acts as a single unit, i.e., combined section properties and thermo-mechanical response with no differential displacement between the repair and host within the segment. Soil friction, f_u, is accounted for in the approach. Compatibility between the segments is used to solve the induced load, which then can be used to determine the elongation of Segment B, i.e., the crack/gap opening displacement (COD). The aforementioned assumptions are intended to produce the largest expected deformation at the gap opening and, therefore, establish a conservative estimate of thermally induced displacement.

9.1.3 Full-Scale Specimen

The specimen for full-scale testing was prepared using two 12 in. (305 mm) diameter steel pipe segments, each 60 in. (1520 mm) long. The host pipe segments were set up such that an initial crack opening of 0.5 in. (12.7 mm) is present. The CIPL was then applied inside the host pipe across the initial gap opening, such that the two host pipe segments were joined to create one test specimen. One side of the specimen includes pipe defects along the host pipe, including varying sized holes and "existing" service connections.

9.2 Full-Scale Transverse Test Setup

The specimen was first tested in a four-point bending configuration with a 22-kip (100 kN) actuator. The specimen was centered about the crack opening with distances between supports and load points being 30

in. – 40 in. – 30 in. (762 mm – 1016 mm – 762 mm). At the support and load points along the specimen, testing saddles were attached to distribute applied loads and minimize localized stress concentrations. Table 9.1 reflects the instrumentation. Strain gauges (SGs) were attached at the crown and invert of the host pipe over the middle 40 in. (1016 mm) (maximum moment) span in the vicinity of the crack. Figure 9.4 shows the strain gauges configuration for transverse loading. String potentiometer (SP) stands were fixed to a beam below the specimen and attached to the springline of the host pipe. Linear variable differential transducers (LVDTs) were attached to the same beam as the SPs, and rods were connected to the springline of the host pipe with brackets.

Table 9.1: Instrument description for transverse loading setup

Instrument Location	Local Instrument Name	Descriptions	Channel No.
Strain Gauges			
East, Crown 10 in. from crack edge, Axial	SG10E_CA	On steel host pipe, crown, east side 10 in. from crack edge	Ch 0
East, Crown, 5 in. from crack edge, Axial	SG5E_CA	On steel host pipe, crown, east side 5 in. from crack edge	Ch 1
East, Crown, 1 in. from crack edge, Axial	SG1E_CA	On steel host pipe, crown, east side 1 in. from crack edge	Ch 2
West, Crown, 1 in. from crack edge, Axial	SG1W_CA	On steel host pipe, crown, west side 1 in. from crack edge	Ch. 3
West, Crown, 5 in. from crack edge, Axial	SG5W_CA	On steel host pipe, crown, west side 5 in. from crack edge	Ch. 4
West, Crown 10 in. from crack edge, Axial	SG10W_CA	On steel host pipe, crown, west side 10 in. from crack edge	Ch. 5
East, Invert 10 in. from crack edge, Axial	SG10E_IA	On steel host pipe, invert, east side 10 in. from crack edge	Ch. 6
East, Invert, 5 in. from crack edge, Axial	SG5E_IA	On steel host pipe, invert, east side 5 in. from crack edge	Ch. 7
East, Invert 1 in. from crack edge, Axial	SG1E _IA	On steel host pipe, invert, east side 1 in. from crack edge	Ch. 8
West, Invert, 1 in. from crack edge, Axial	SG1W_IA	On steel host pipe, invert, west side 1 in. from crack edge	Ch. 9
West, Invert, 5 in. from crack edge, Axial	SG5W_IA	On steel host pipe, invert, west side 5 in. from crack edge	Ch. 10
West, Invert, 10 in. from crack edge, Axial	SG10W_IA	On steel host pipe, invert, west side 10 in. from crack edge	Ch 11
East, Crown, 1 in. from crack edge, Circumferential	SG1E_CC	On steel host pipe, crown, east side 1 in. from crack edge	Ch 12
West, Crown, 1 in. from crack edge, Circumferential	SG1W_CC	On steel host pipe, crown, west side 1 in. from crack edge	Ch 13
East, Invert, 1 in. from crack edge, Circumferential	SG1E_IC	On steel host pipe, invert, east side 1 in. from crack edge	Ch 14
West, Invert, 1 in. from crack edge, Circumferential	SG1W_IC	On steel host pipe, invert, west side 1 in. from crack edge	Ch15
Actual String Pots			
Far East 16 in. From crack edge on the south side of pipe	SP FE [SP23-3]	On steel host pipe, east side, south springline, 16 in. from crack edge	SP0 Ch. 0

Near East 2.5 in. From crack edge on the south side of pipe	SP E [SP29-10]	On steel host pipe, east side, south springline, 2.5 in. from crack edge	SP1 Ch. 1
Near West 2.5 in. From crack edge on the south side of pipe	SP W [SP24-10]	On steel host pipe, west side, south springline, 2.5 in. from crack edge	SP2 Ch. 2
Far West 16 in. From crack edge on the south side of pipe	SP FW [SP22-10]	On steel host pipe, west side, south springline, 16 in. from crack edge	SP3 Ch. 3
LVDTs			
Far West From crack edge, Invert, 25 in	LVDT FW [SN1005]	On bracket on steel, far West, invert, outside West load saddle, 25 in from crack edge	LVDT Ch. 0
Near West From crack edge, Invert, 1.5 in	LVDT W [SN1016]	On backet on steel, Wast, invert, 1.5 in. from crack edge	LVDT Ch. 1
Near East From crack edge, Invert, 1.5 in	LVDT E [SN1021]	On backet on steel, East, invert, 1.5 in. from crack edge	LVDT Ch. 2
Far East From crack edge, Invert, 25 in	LVDT FE [SN1008]	On bracket on steel, far East, invert, outside East load saddle, 25 in from crack edge	LVDT Ch. 3
MTS			
MTS Actuator Piston Position	Applied Force	MTS Crosshead (Above Specimen)	
MTS Actuator Piston Position	Applied Displacement	MTS Crosshead (Above Specimen)	
150 psi Pressure Transducer	End cap	End cap	Ch. 20

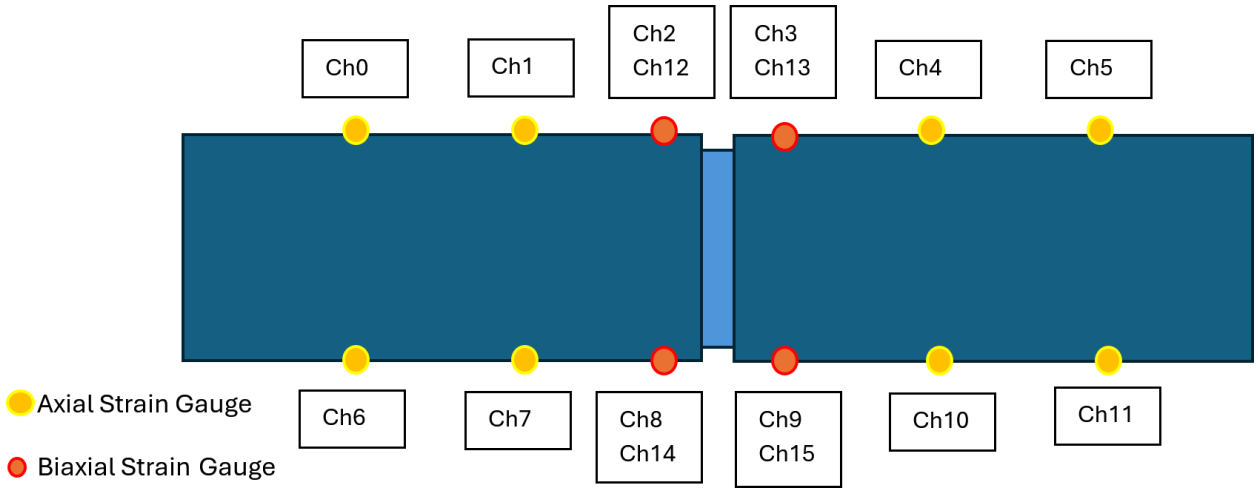

Figure 9.4: Strain Gauge configuration for transverse loading setup

Figure 9.5 shows a photo of the full-scale specimen in the frame prior to testing. Figure 9.6 provides a schematic for the instrumentation with detailed dimensions.

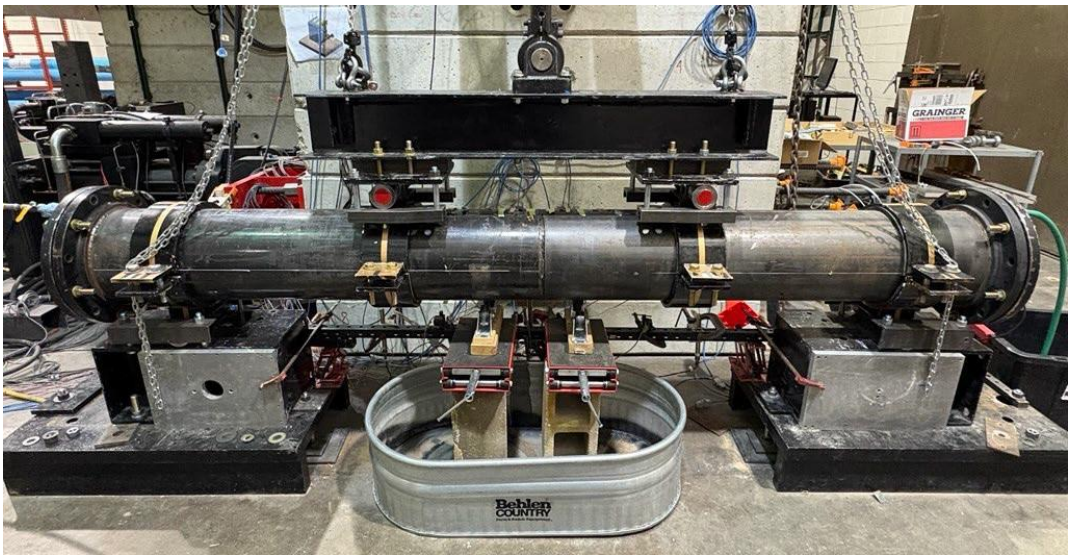

Figure 9.5: Full-scale specimen in frame with four-point bending configuration

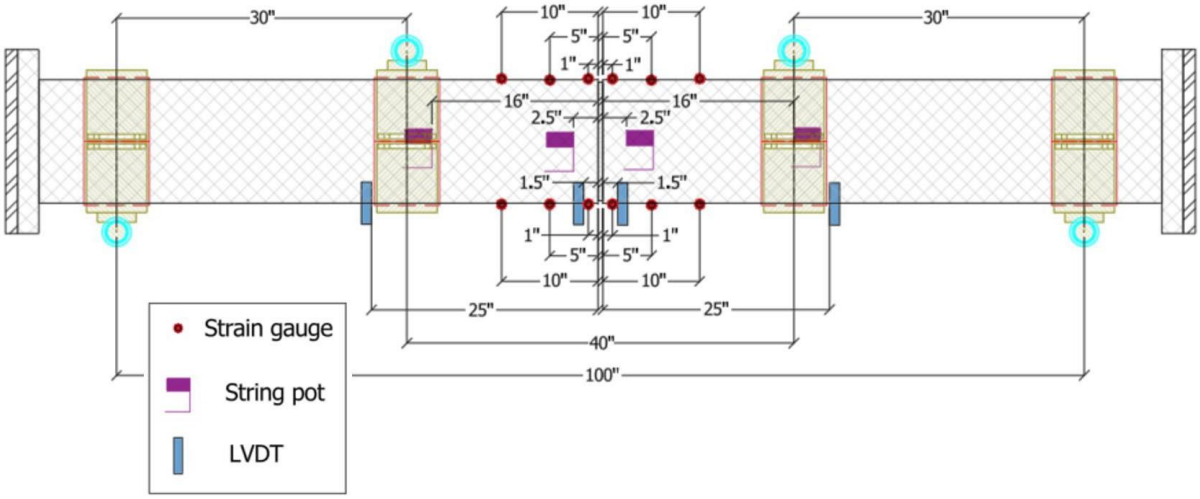

Figure 9.6: Full-scale test instrumentation schematic

Several preliminary bend tests were performed on SL01 to check that instrumentation was functioning and assess the stiffness. Traffic loading cycles were then performed. These were predominantly performed at cyclic frequencies of 1 Hz and 2 Hz, associated with sample rates of 64 Hz and 128 Hz, respectively. For SL01, the targeted rotation was 0.11°, which was determined from the analysis as described in Section 9.1.1.2. Applied global rotations ranged from 0.09° to 0.12°; the actuator displacement associated with achieving these rotations was about 0.044 in from the LVDTs close to the gap opening.

Most traffic cycles were performed with constant dead water pressure at 65 psi. However, the first 100K cycles were performed at 10 psi, then next 100K cycles at 30 psi. With these pressures, similar rotations were achieved with similar actuator displacements.

Then deformations were applied to simulate adjacent (i.e., parallel) excavations. These were performed with constant live internal water pressure, which led to pressure fluctuations under large deformation. Cages were loosened and restraining chains were loosened for this procedure. This consisted of an initial bend to a rotation of 0.65°, associated with an actuator displacement of 0.27 in. The actuator was then returned to the initial test position, and the specimen was loaded to a rotation of 1.29°, associated with an actuator displacement of 0.54 in. These rotations correspond to values from the adjacent excavation model considering soil displacements of 2.5 in. and 5 in. Crosshead speed was 0.2 in./min (5 mm/min).

After the adjacent excavation testing, the cages were retightened. Roughly 100,000 subsequent traffic cycles were then performed with similar rotation about the gap and actuator displacement as the previous cycles. All SL01 pressurizations and depressurizations were recorded with 16 Hz sampling rate. When not under test, the specimen was kept in a depressurized state.

1. 9.3 Full-scale Transverse Test Results

The full-scale specimen was first subjected to 500,000 transverse loading cycles representative of traffic loads. A sinusoidal displacement wave was applied to achieve different target rotations over the duration of the test. The specimen was tested with dead pressure. Initial cycles started at 10 psi, as traffic cycles progressed internal pressure was increased to 30, then 65 psi. A target transverse displacement of 0.048 in. was applied to achieve a target rotation of 0.114°. The moment required to reach this rotation was 37 kip-in. (4.1 kN-m) towards the beginning of traffic cycles. The internal pressure was increased over the first 180k cycles and was held at 65 psi for the following 300k cycles. Table 9.2 tracks the changes in testing parameters. The apparent stiffness decreased from approximately 435 kip-in./deg (49.1 kN-m/deg) to 220 kip-in./deg (24.8 kN-m/deg) as testing progressed. Figure 9.7 shows the moment versus rotation for the specimen as testing progressed, plot (a) compares behavior of the IRP every 100,000 cycles and plot (b) looks at only 2 cycles, one from the start of test BC07 and one from the start of test BC08. While both plots show a change in apparent stiffness as testing progressed, plot (b) shows how much apparent stiffness decreased when internal pressure of SL01 increased from 30 psi to 65 psi. The change in stiffness was likely due to some debonding that occurred during the first cycles at a higher internal pressure. Popping noises were heard during the start of the test, which is an indication of this behavior.

Table 9.2: Testing details for SL01 traffic cycles

Test ID	Cycle Range	Internal Pressure (psi)	Sampling Rate (Hz)	Target Rotation (deg)	Target Displacement (in.)
BC-initial	1	10	1	0.052	0.022
BC01 – BC02	2 – 5.3k	10	1	0.069	0.029
BC03	5.4k – 17.3k	10	1	0.114	0.048
BC04 – BC05	17.4k – 100k	10	2	0.114	0.048
BC06 – BC07	101k – 180k	30	2	0.114	0.048
BC08 – BC15	181k – 500k	65	2	0.114	0.048

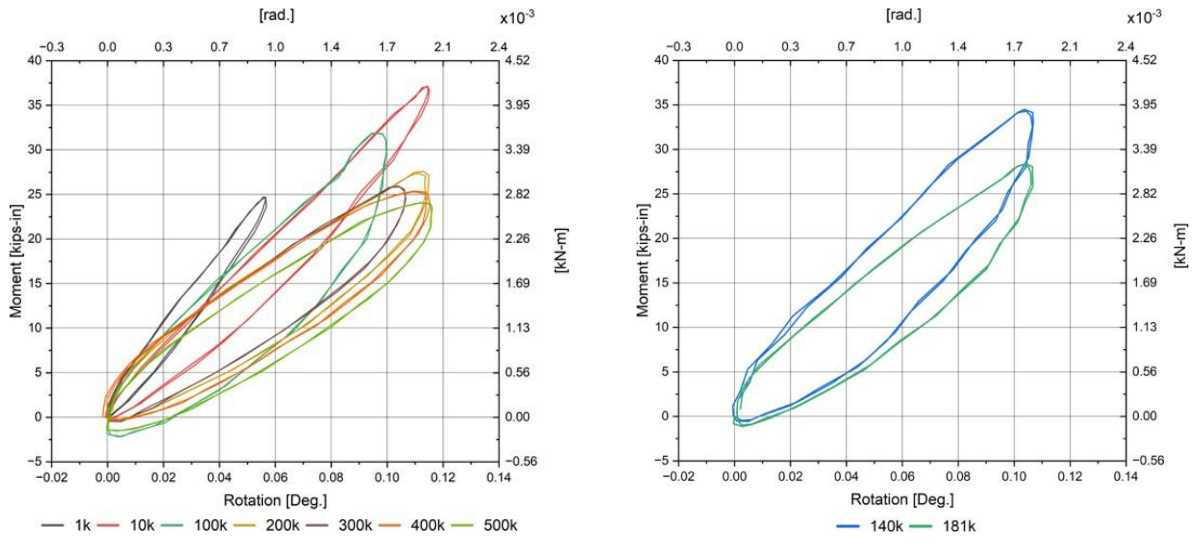

(a) **(b)**

Figure 9.7: Moment vs rotation for selected traffic cycles (a) throughout the first 500,000 traffic loading cycles and (b) before and after increasing internal pressure

After 500,000 traffic loading cycles were completed, two larger transverse displacements were applied to SL01 to represent parallel excavation (PE) events in the field. Target rotations of 0.697° and 1.373° were calculated to simulate smaller and larger events, which translated to target displacements of 0.292 in. and 0.575 in., respectively. Before the second target displacement was reached during the second parallel excavation event (PE02), large chunks of resin on the crown of the specimen popped off the liner at the crack. This decreased the stiffness at the gap opening, which allowed the specimen to experience more displacement. Figure 9.8 shows the moment versus rotation curves for the parallel excavation events. Because of the change in stiffness mid-push, a third PE test was run with an updated target rotation and displacement of 1.395° and 0.584 in., included in Figure 9.8. Figure 9.9 shows a photo of the gap opening of SL01 before and after the second parallel excavation event.

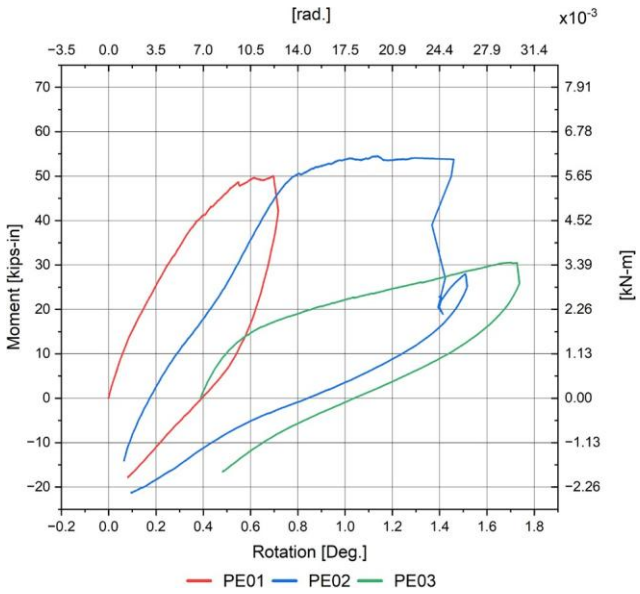

Figure 9.8: Moment vs rotation for SL01 parallel excavation events

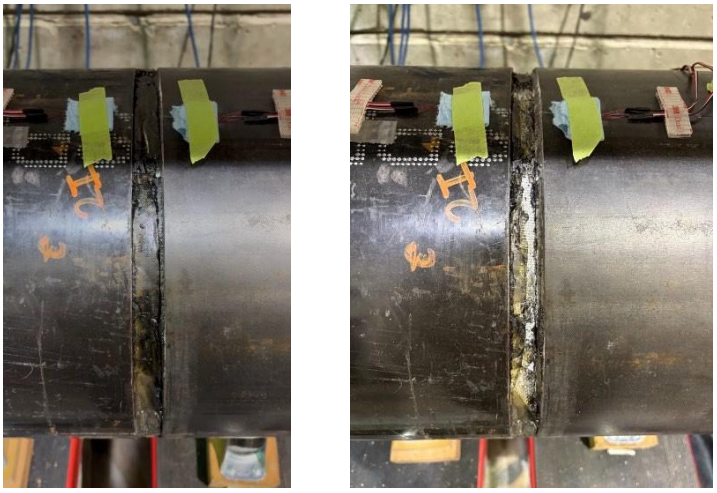

(a) **(b)**

Figure 9.9: Photo of SL01's gap opening (a) before and (b) after the first two parallel excavation events

After the parallel excavation events, an additional 100,000 traffic loading cycles were applied at 65 psi to the specimen. The target rotation and displacement were updated to be 0.123° and 0.052 in., respectively. The specimen reached a moment of 16.2 kip-in. (1.8 kN-m) to reach the desired targets. The approximate stiffness of the specimen at the end of transverse testing was measured to be 137 kip-in./deg (15.4 kN-m/deg). Compared to the value of 432 kip-in./deg (48.8 kN-m/deg) measured after 1,000 cycles, the approximate stiffness of SL01 decreased by 68%.

9.4 Full-Scale Axial Test Setup

After transverse loading was completed, the specimen was subjected to total of 68 axial cycles. 50 cycles of axial loading were conducted to represent the thermal expansion due to temperature fluctuations in the soil. 9 pre-test and 9 post-test axial cycles at 0, 30, and 60 psi were conducted (each 3 cycles) to study the internal pressure effects. The specimen was carefully moved to a rigid self-containing frame where a 110-kip (500 kN) actuator with an 11 in. (280 mm) stroke was used to perform axial cycles. Table 9.3 reflects the instrumentation for axial loading setup. Strain gauge (SG) locations remained the same as the previous transverse testing. One SG was added directly to the liner at the crack opening where resin had broken off in the parallel excavation test. Three SPs were set up along the north shoulder, south haunch and south springline of the specimen, fixed to the steel host pipe, spanning the crack opening. Three LVDTs were set up similar to the SPs, though at the crown, invert and north springline of the specimen. Displacement sensors were set up such that the crack opening displacement (COD) could be monitored during axial cycles. For ultimate pull test four SGs were added on the liner (after AC15) and replaced with SGs on host pipe (has shown in red in Table 9.3). Figure 9.10 shows a photo of the full-scale specimen in the frame prior to testing. Figure 9.11 provides a schematic for the instrumentation with detailed dimensions.

Table 9.3: Instrument description for axial loading setup

Instrument Description	Local Instrument Name	Location	Channel No.
Strain Gauge			
East, Crown 10 in. from crack edge, Axial	SG10E_CA	On steel host pipe, crown, east side 10 in. from crack edge	Ch 1
East, Crown, 5 in. from crack edge, Axial	SG5E_CA	On steel host pipe, crown, east side 5 in. from crack edge	Ch 2
East, Crown, 1 in. from crack edge, Axial	SG1E_CA	On steel host pipe, crown, east side 1 in. from crack edge	Ch. 3
West, Crown, 1 in. from crack edge, Axial	SG1W_CA	On steel host pipe, crown, west side 1 in. from crack edge	Ch. 4
West, Crown, 5 in. from crack edge, Axial	SG5W_CA	On steel host pipe, crown, west side 5 in. from crack edge	Ch. 5
West, Crown 10 in. from crack edge, Axial	SG10W_CA	On steel host pipe, crown, west side 10 in. from crack edge	Ch. 6
East, Invert 10 in. from crack edge, Axial	SG10E_IA	On steel host pipe, invert, east side 10 in. from crack edge	Ch. 7
East, Invert, 5 in. from crack edge, Axial	SG5E_IA	On steel host pipe, invert, east side 5 in. from crack edge	Ch. 8
East, Invert 1 in. from crack edge, Axial	SG1E _IA	On steel host pipe, invert, east side 1 in. from crack edge	Ch. 9
West, Invert, 1 in. from crack edge, Axial	SG1W_IA	On steel host pipe, invert, west side 1 in. from crack edge	Ch. 10
Centerline, south haunch, 0 in from crack edge, Circumferential	SG0L_SHC	On liner, south haunch, centerline 0 in. from crack edge	Ch. 10
West, Invert, 5 in. from crack edge, Axial	SG5W_IA	On steel host pipe, invert, west side 5 in. from crack edge	Ch 11
West, Invert, 10 in. from crack edge, Axial	SG10W_IA	On steel host pipe, invert, west side 10 in. from crack edge	Ch 12
East, Crown, 1 in. from crack edge, Circumferential	SG1E_CC	On steel host pipe, crown, east side 1 in. from crack edge	Ch. 13
West, Crown, 1 in. from crack edge, Circumferential	SG1W_CC	On steel host pipe, crown, west side 1 in. from crack edge	Ch. 14
East, Invert, 1 in. from crack edge, Circumferential	SG1E_IC	On steel host pipe, invert, east side 1 in. from crack edge	Ch. 15
West, Invert, 1 in. from crack edge, Circumferential	SG1W_IC	On steel host pipe, invert, west side 1 in. from crack edge	Ch. 16
Centerline, north haunch, 0 in. from crack edge, Axial	SG0L_NHA	On liner, north haunch, centerline 0 in. from crack edge	Ch. 16

Centerline, Crown, 0 in. from crack edge, Axial	SG0L_CA	On liner, crown, centerline 0 in. from crack edge	Ch. 17
Centerline, North Haunch, 0 in. from crack edge, Circumferential	SG0L_NHC	On liner, north haunch, centerline 0 in. from crack edge	Ch. 17
Centerline, Crown, 0 in. from crack edge, Circumferential	SG0L_CC	On liner, crown, centerline 0 in. from crack edge	Ch. 18
West, Invert, 1 in. from crack edge, Circumferential	SG1W_IC	On steel host pipe, invert, west side 1 in. from crack edge	Ch. 19
Centerline, South Haunch, 0 in. from crack edge, Axial	SG0L_SHA	On liner, south haunch, centerline 0 in. from crack edge	Ch. 19
String Potentiometer			
North Shoulder, Over crack, Fixed to west steel pipe	SP18-10_NSh	West side, North shoulder, line spans over the crack axially	Ch. 21
South Haunch, Over crack, Fixed to west steel pipe	SP07-20_SH	West side, South haunch, line spans over the crack axially	Ch. 22
South Springline, Over crack, Fixed to west steel pipe	SP22-10_SS	West side, South springline, line spans over the crack axially	Ch. 23
North side of pipe perpendicular to the axial frame to measure buckling	SP39-10_NB	North side on frame, East springline, line spans perpendicular to pipe	Ch. 26
LVDTs			
LVDT SN1005, East Side/Center, Crown, 1.5 in from crack edge	LVDT05_1005EC	On backet on steel, east, crown, 1.5 in. from crack edge	LVDT Ch. 1
LVDT SN1008, East Side/Center, Invert, 1.5 in from crack edge	LVDT08_1008EI	On backet on steel, east, invert, 1.5 in. from crack edge	LVDT Ch. 4
LVDT SN1017 East Side/Center, North Springline, 1.5 in from crack edge	LVDT17_1017NSP	On backet on steel, east, North Springline, 1.5 in. from crack edge	LVDT Ch. 6
Pressure Gauge			
150 psi Pressure Transducer	PT_omega15	pressurization pump	Ch. 20
100 psi Pressure Transducer	PT_omega10	East end cap	Ch. 25
Actuator			
MTS Actuator Piston Force	110-kip	MTS Crosshead (Above Specimen)	
MTS Actuator Piston Position		MTS Crosshead (Above Specimen)	

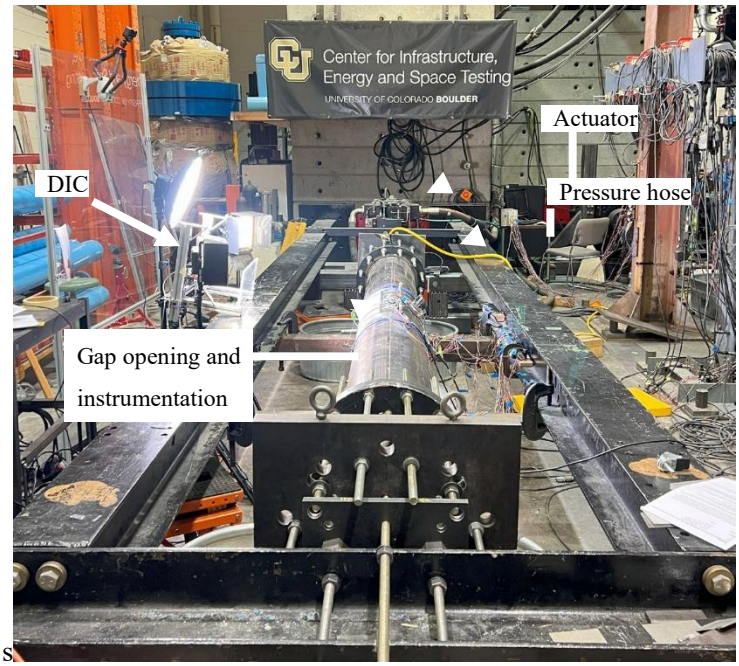

Figure 9.10: Full-scale specimen in axial loading frame

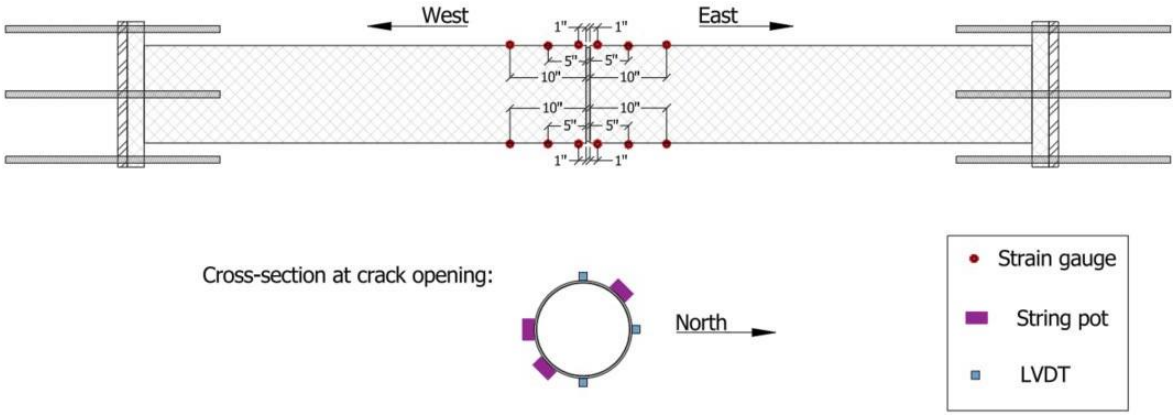

Figure 9.11: Full-scale axial test instrumentation schematic

9.5 Full-Scale Axial Test Results

Figure 9.12 presents the applied actuator displacement, actuator force and average LVDT measurements relative to time for each cycle applied. Figure 9.13 shows the load relative to the gap/crack opening displacement (COD) for the selected axial cycles. The COD is the average of the LVDTs located at the crown and invert.

Several preliminary cycles with relatively small target displacements were conducted to measure the specimen's initial stiffness. During the initial cycle, the actuator applied a displacement that generated approximately 7.4 kips (33 kN) of tensile force, resulting in a measured COD of 0.025 in. (0.635 mm). From these measurements, an initial stiffness of approximately 301.5 kip/in. (52.8 kN/mm) was calculated. This stiffness was then used to calculate the target COD for the subsequent cycles. As the testing progressed, the target COD increased because the apparent stiffness from each set of cycles was used to adjust the target displacement for the following set. In the early cycles, the stiffness was calculated to be around 69.6 kip/in. (12.2 kN/mm). By cycle 50, the average stiffness dropped to 60.4 kip/in. (10.6 kN/mm), indicating a reduction of about 13% from the earlier cycles.

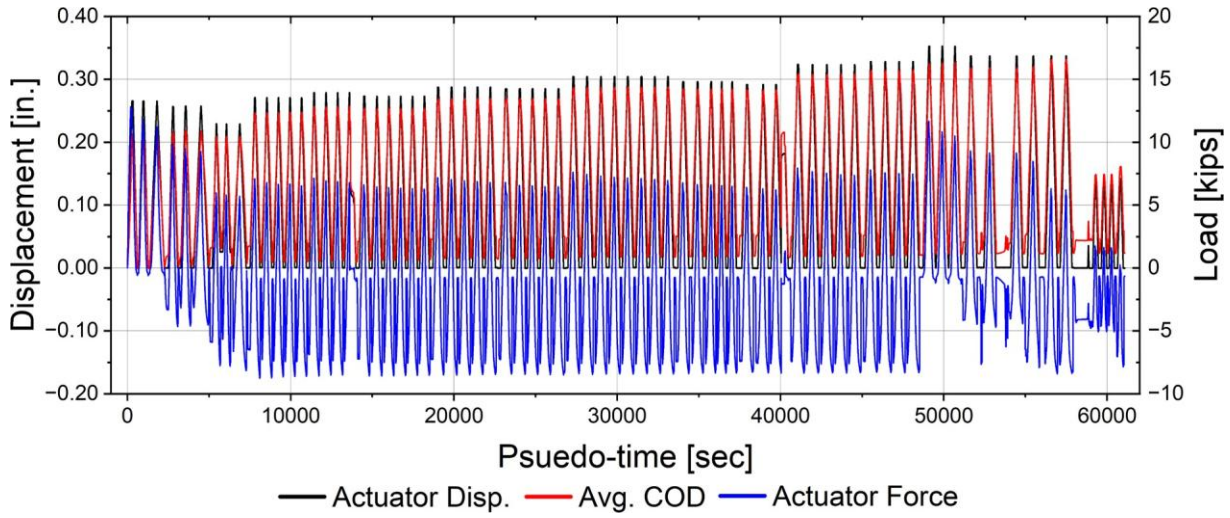

Figure 9.12: Actuator displacement, actuator force, and average LVDT measurements vs. time for axial cycles

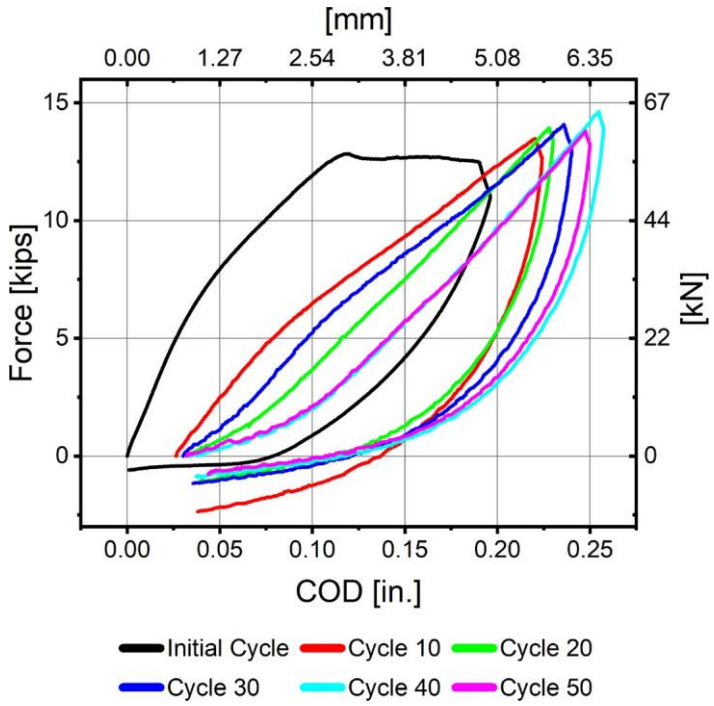

Figure 9.13: Actuator load vs. crack opening displacement (COD) for various axial cycles

Figure 9.14 shows the load relative to the gap/crack opening displacement (COD) for representative cycles at varying internal pressures (0psi, 30psi, 60psi). The data are shown for cycles 1-50 and for cycles performed after the first 50.

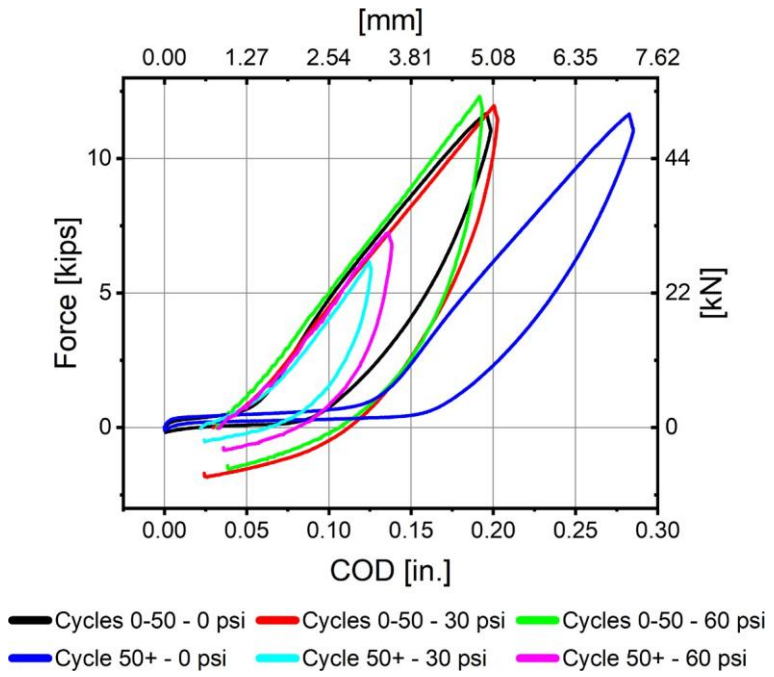

Figure 9.14: Actuator load vs. crack opening displacement (COD) at various internal pressures before and after 50 cycles

Once thermal expansion cycles were completed, the specimen was axially loaded to its ultimate capacity with an internal pressure of 60psi. At loads of about 18 kips (80 kN), debonding of the IRP started, with debonding events occurring at intervals of about 15 to 80 seconds. The specimen reached a peak ultimate force capacity of about 29.5 kips (131 kN) at a COD of about 5.1 in. (129 mm). At this point, rupture in the IRP occurred, ending the test. Figure 9.15 shows the actuator force and displacement measured by the string pots and LVDT's, where the jumps in force correspond to debonding events. Several of the LVDTs had a maximum measurement range of 2 in., after which their values are inaccurate, while the string pots were able to capture the entire COD displacement progression, with each measurement reaching approximately 5 in. of displacement (SP Buckling was a transverse measurement that was not measuring COD). The apparent stiffness was approximately 51.3 kips/in. (9.0 kN/mm). No leakage occurred prior to failure. Figure 9.16 shows the specimen in the axial frame before and after failure from north and south views, illustrating the shift from distributed axial deformation to damage concentrated at the gap region.

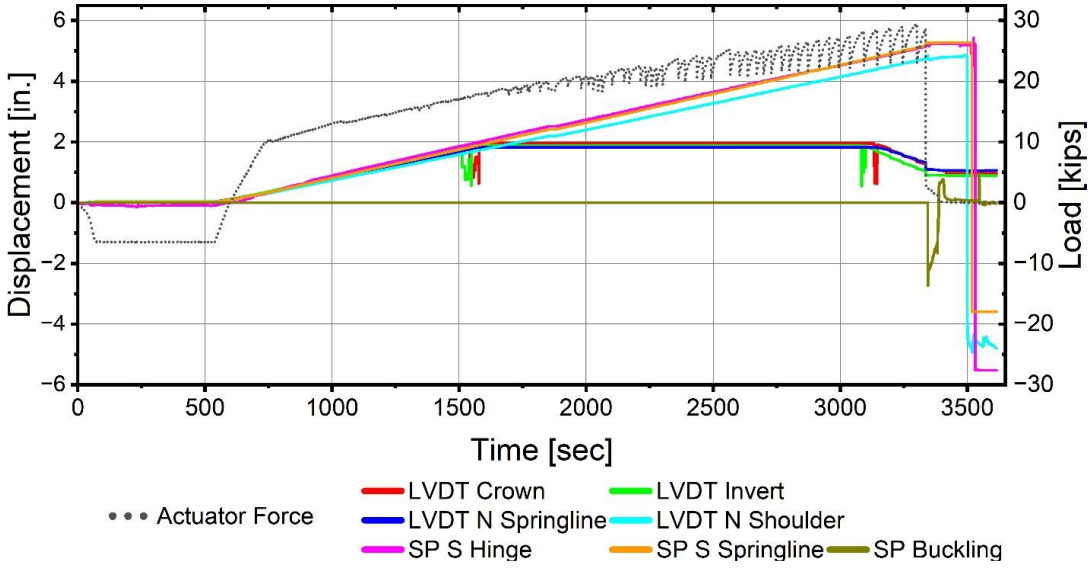

Figure 9.15: Actuator force and string pot displacement vs. time for ultimate axial tension test

a)

b)

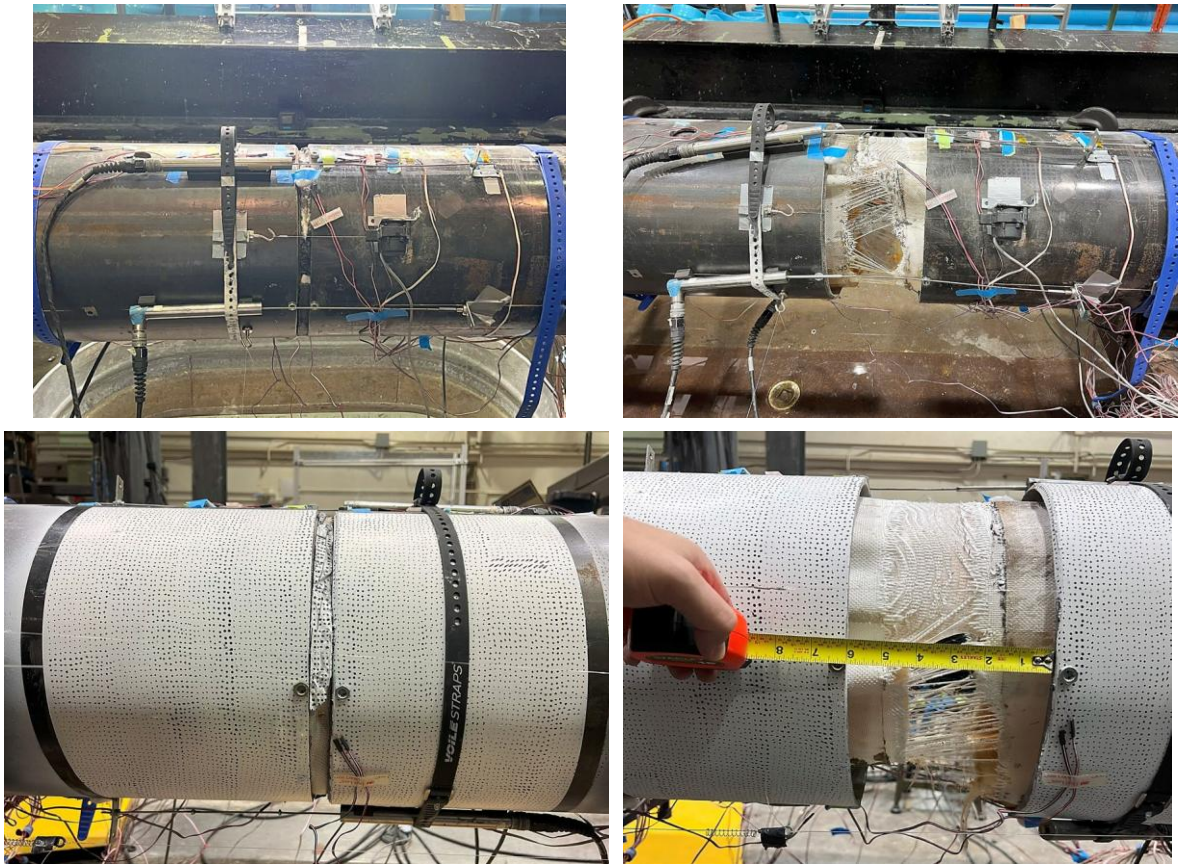

Figure 9.16: Specimen in the axial loading frame, before (left) and after (right) ultimate pull test: (a) North view; (b) South view.

7. Conclusions

For the first part of testing plan, at least eight coupons were tested per chemical and pipe material type during chemical tests in accordance with Testing Method D543 Procedure B. Less than 5% change in dimensions and weight was reported in every category except liner thickness, which could possibly be due to measuring error of the very small thickness values. The chemically tested coupons were then used in mechanical testing. Peel testing was conducted in accordance with Testing Method D3167, hardness testing was done in accordance with Testing Method D2240, and lap shear tests were done in accordance with Test Method D5868. The average peel strength of all coupons was 8.58 lbf/in (1.50 N/mm), the average hardness was 47.1D, and the average lap shear peak stress was 89.6 psi (617.4 kPa). The peel tests reported were all over 6 lb/in (1.05 N/mm), in accordance with ASTM F2207 Section 5.2.2.1.

This section summarizes the findings of the testing program performed on 12-in.- (300-mm) diameter specimens repaired with STARLINE2000™ internal replacement pipe (IRP). The specimen was prepared with a nominal 0.5-in. (12.7 mm) of exposed STARLINE2000™ lining, with approximately 5 ft (1.52 m) of steel host pipe on either side of the gap. It was subjected to cyclic transverse and axial loading using specialized testing equipment at the Center for Infrastructure, Energy, and Space Testing (CIEST) at the University of Colorado Boulder.

The general methodology consisted of applying bending deformation to a pipe specimen, followed by axial loading. Bending involved 500,000 short duration (1 to 2 Hz) cycles representing cyclic deformation caused by surface traffic. This fatigue testing was followed by larger bending deformations reflective of the system responses to adjacent excavation activity, which in turn were followed by roughly 100,000 additional “traffic” cycles. Then, over 50 axial cycles were applied, representing the thermal deformation over 50 years associated with annual temperature changes, ΔT, of 40°F or 50°F (22.2°C or 27.8°C). Final axial tension test was performed to assess the ultimate pullout capacity of the host pipe with STARLINE2000™ IRP. As prescribed by the test program, the ultimate capacity in axial tension was achieved at an axial force of approximately 29.5 kips (131 kN) and with a gap opening displacement at failure of roughly 5.1 in. (130 mm). Most testing was performed at about 65 psi (450 kPa) of internal water pressure.

The levels of excavation movement assumed for the adjacent excavation cycles were associated 2.5 in. (63.5 mm) and 5 in. (127 mm) for the small and large events, respectively. The 5 in. (127 mm) level of soil displacement is expected to be used to set maximum parallel excavation deformation levels in future studies. The targeted rotational deformations depend on the stiffness of the repair pipe and the nature of the

bonding between the repair and host pipe. If another IRP technology had a similar stiffness to STARLINE2000^{TM}, similar deformation levels would be anticipated. Initial stiffness tests of specimens and comparison with analytical and/or numerical models will inform the degree of bonding and, thus, deformation levels (for example see Klingaman et al., 2024).

The apparent bending stiffness of the specimen, using a global rotation calculated from LVDTs positioned just outside the load points, decreased over the 500,000 traffic-type cycles from approximately 435 kip-in./deg to 220 kip-in./deg (49 to 25 kN-m/deg) as internal pressure was stepped from 10 to 30 to 65 psi. A target transverse displacement of 0.048 in. produced a target rotation of 0.114°, requiring a moment of about 37 kip-in. (4.1 kN-m) near the start of cycling. The most pronounced stiffness reduction occurred after the increase to 65 psi, consistent with limited de-bonding indicated by audible "popping" at the outset of the test. Throughout the transverse (bending) loading, the specimen did not become structurally compromised and maintained water containment.

The axial load stiffness associated with the initial practice cycle was approximately 302 kip/in. (52.8 kN/mm), based on a tensile force of ~7.4 kips at a COD of 0.025 in. (COD averaged from crown and invert LVDTs). As cycling progressed, the apparent stiffness reduced to ~69.6 kip/in. (12.2 kN/mm) in the early cycles and to ~60.4 kip/in. (10.6 kN/mm) by Cycle 50—about a 13% decrease relative to the early cycles and roughly an 80% reduction from the initial small-displacement estimate.

Target CODs for subsequent cycles were determined iteratively from the measured stiffness (rather than from a pre-set analytical safety factor), and cycles were performed at internal pressures of 0, 30, and 60 psi. After completing the thermal expansion cycles, the specimen was pulled in axial tension at 60 psi: debonding initiated near 18 kips (80 kN) and the peak capacity reached 29.5 kips (131 kN) at a COD of 5.1 in. (129 mm). The corresponding apparent (secant) stiffness near peak was 51 kip/in. (9.0 kN/mm). No leakage occurred prior to failure.

The STARLINE2000^{TM} repair system performed well under all applied external loads representative of 50 years of service. No cracks or significant structural damage to the IRP were observed during service life testing, and no leakage occurred until ultimate capacity was reached. The product was able to debond locally from the host pipe to accommodate strain concentrations while achieving containment and continuity. While this testing program and the applied cycles were limited to a 50-year service life due to project time constraints, the performance observed suggests that longer durations of testing could demonstrate the ability of the system to accommodate additional years of mechanical aging. This research

demonstrates that the proposed service life testing procedures can be accommodated by an existing trenchless technology and supports further applications of the proposed methods.